

Transversal optical singularity induced precision measurement of step-nanostructures

Dou, Xiuji; Zhou, Jiakang; Zhang, Yuquan; Min, Changjun; Pereira, S. F.; Yuan, Xiaocong

DOI

[10.1364/OE.500909](https://doi.org/10.1364/OE.500909)

Publication date

2023

Document Version

Final published version

Published in

Optics Express

Citation (APA)

Dou, X., Zhou, J., Zhang, Y., Min, C., Pereira, S. F., & Yuan, X. (2023). Transversal optical singularity induced precision measurement of step-nanostructures. *Optics Express*, 31(20), 32840-32848. <https://doi.org/10.1364/OE.500909>

Important note

To cite this publication, please use the final published version (if applicable). Please check the document version above.

Copyright


Other than for strictly personal use, it is not permitted to download, forward or distribute the text or part of it, without the consent of the author(s) and/or copyright holder(s), unless the work is under an open content license such as Creative Commons.

Takedown policy

Please contact us and provide details if you believe this document breaches copyrights. We will remove access to the work immediately and investigate your claim.



Transversal optical singularity induced precision measurement of step-nanostructures

XIUJIE DOU,^{1,2}  JIAKANG ZHOU,² YUQUAN ZHANG,² CHANGJUN MIN,^{2,*} S. F. PEREIRA,¹ AND XIAOCONG YUAN²

¹Optics Research Group, Department of Imaging Physics, Faculty of Applied Sciences, Delft University of Technology, Lorentzweg 1, 2628 CJ Delft, The Netherlands

²Nanophotonics Research Centre, Institute of Microscale Optoelectronics & State Key Laboratory of Radio Frequency Heterogeneous Integration, Shenzhen University, Shenzhen 518060, China

*cjmin@szu.edu.cn

Abstract: Optical singularities indicate zero-intensity points in space where parameters, such as phase, polarization, are undetermined. Vortex beams such as the Laguerre–Gaussian modes are characterized by a phase factor $e^{i\ell\theta}$, and contain a phase singularity in the middle of its beam. In the case of a transversal optical singularity (TOS), it occurs perpendicular to the propagation, and its phase integral is 2π in nature. Since it emerges within a nano-size range, one expects that TOSs could be sensitive in the light-matter interaction process and could provide a great possibility for accurate determination of certain parameters of nanostructure. Here, we propose to use TOSs generated by a three-wave interference to illuminate a step nanostructure. After interaction with the nanostructure, the TOS is scattered into the far field. The scattering direction can have a relation with the physical parameters of the nanostructure. We show that by monitoring the spatial coordinates of the scattered TOS, its propagation direction can be determined, and as consequence, certain physical parameters of the step nanostructure can be retrieved with high precision.

© 2023 Optica Publishing Group under the terms of the [Optica Open Access Publishing Agreement](#)

1. Introduction

With continuing miniaturization and intelligence of optoelectronic devices and the explosive demand of the consumption market, the semiconductor industry advances towards higher-level products that need to be made in shrinking critical size and high volume, which also puts forward higher requirements for metrology methods [1]. To ensure the functionality and yield of the semiconductor chips, quality assessment is always an important topic in the modern manufacturing industry. Optical scatterometry [2–4] has been used extensively in the manufacturing process, and it has shown sufficient robustness in the in-line process quality control and sufficient accuracy in critical dimension measurement. For the next generation of lithography, in addition to the critical dimension of micro/nanostructures, more accurate measurements need to be executed to reduce the uncertainties of the determination of side-wall angle (SWA), the surface roughness and the left/right round corners of the nanostructures. Furthermore, we identified that SWA is one of the least predicable and controllable parameters in the chip manufacturing process. Quality assessment is still a very challenging and urgent matter. The conventional optical scatterometry usually uses the amplitude, the polarization and in some cases the phase characteristics of the scattered light to determinate the parameters of the target structure. However, with the further exploration of light properties, other characteristics such as singularity [5], orbital angular momentum [6], spin angular momentum [7] also show great potential to improve such parameter determination.

Optical singularity is an undefined physical point in optical field [8–11]. It always leads to a zero-field intensity and possesses a high gradient in an ultra-tiny region around the singularity. There are two main forms of optical singularities: the polarization and phase versions; both have

been widely employed in many frontier research and application areas [12–15]. The polarization singularity, which appears widely in vector beams, has been demonstrated to achieve extreme sensitivity in detecting slight changes due to the interaction with (nano)objects [16,17]. The phase singularities are ubiquitous in complex wave systems and typically arise due to discontinuous phase variation. In optical vortex beams, the helical phase circulates around a zero-field point, thus generate an orbital angular momentum (OAM) to form an optical phase singularity. The phase integration around an OAM is an integer multiple of 2π , being known as the topological charge (TC). Physically, the phase singularities can be divided into the longitudinal and transversal states, i.e., parallel and perpendicular to the propagation, respectively. For the longitudinal optical singularity (LOS), it possesses an arbitrary TC, which induces LOS always acting in a relatively broad range, usually in the size of several wavelengths, due to its sufficiently small wave vector decomposed in the light field transverse section. LOS has been widely used in optical interconnection, computing, and optical manipulation areas [9,18–20]. In the case of transversal optical singularity (TOS), however, the phase integration around the singularity is 2π in nature, and always emerges within the range of one wavelength. The above-mentioned TOS is a pure spatial beam mode without considering changes in the temporal domain. Very recently, the generation of light with spatiotemporal TOS has been demonstrated both in theory and experiment [21–26]. It provides an additional temporal freedom, which it is expected to have impact in frontier research.

It has been shown that TOS occurs at the nodal lines with complete destructive interference as for example edge diffraction [27], interference of Gaussian beams [28], under highly focusing condition [29], or multiple plane waves overlapping in space [30–32]. Here, we employ three linearly polarized Gaussian waves with intersection angle of 0° and $\pm 45^\circ$ to generate an array of TOSs in the interference region. After the interaction with the step nanostructure, the scattering field also contains phase singularities and is detectable in the far field. We have seen that the scattering direction depends highly on the parameters of the step-structure. By detecting the scattering angle of the scattered TOS, the height and SWA of the structure can be reconstructed with high precision. The numerical results demonstrate that this is an efficient and sensitive method, and it provides a good complement to coherent Fourier scatterometry technique for finer measurements of nanostructures.

2. Principles and methods

It has been demonstrated that three plane waves are sufficient to produce transversal phase singularities [33–35]. The three-wave interference always results in an array of vortices, as long as sum of the two smallest phasors exceeds the amplitude of the largest one [31]. Here, without loss of generality, we consider the generation of TOSs by three Gaussian beams interference, where the beams have equal amplitude and the same polarization direction, i.e., the y-axis direction in our case. The three Gaussian waves are placed in the same x-z plane and symmetric with the z-axis (see Fig. 1(a)), with waist radius of $1.02\ \mu\text{m}$, equivalent to the case of a focused beam with NA of 0.2. The interference field forms an array of TOSs. As the three waves are distributed symmetrically with z-axis, the TOSs are also axially symmetric. The distribution of the TOSs can be modulated by the wavelength and the angle of the incident waves, the influences of these two factors have been discussed in the [Supplement 1](#). Here, the wavelength of the incident waves is chosen at 633 nm and their propagation angles are set as 0° and $\pm 45^\circ$ with z-axis, respectively. Figure 1(b) and 1(c) are the field intensity and phase distribution of the interference field, respectively. TOSs are essentially the same in physical properties. Hereinafter, we will focus on a randomly selected TOS (labeled in Fig. 1(c) by a blue circle) to investigate its changes after interacting with the structure.

When the beam is focused on a flat substrate, the original interference field will be redistributed due to the influence of the substrate, as shown in Fig. 1 (d) and (e). The coordinate of the selected

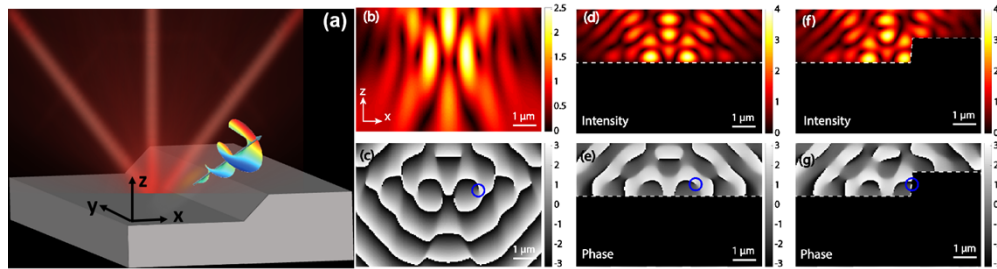


Fig. 1. Scheme of the TOS induced precise detection. (a) Schematic of the TOS generation and its interaction with the silicon-based step nanostructure. The wavelength of the incident beam is 633 nm. (b) and (c) are the intensity and phase distribution of the interference field in a free space. (d) and (f) are the total field after interaction with the flat substrate and the step-structure. (e) and (g) are the phase distribution of the fields corresponding to (d) and (f). The position of the generated TOS is marked by a blue circle. (g) indicates that the TOS interacts with the edge of the step nanostructure.

TOS in Fig. 1(e) needs to be extracted to ensure that the step structure can be accurately placed on this position. The intensity and phase distribution for the interaction between TOS field and the step nanostructure are depicted in Fig. 1(f) and 1(g), respectively. Figure 1(g) indicates that the selected TOS will interact with the step nanostructure. In the interaction process, the original localized TOSs will be scattered into the far field, keeping its transversal characteristic valid in the scattering process [36–38]. It needs a certain propagation distance to retrieve the scattered TOS, thus no TOS is retrieved in Fig. 1(g) (Fig. 1(g) is the phase pattern where $y = 0$). For the scattered TOS, its propagation trajectory line is highly dependent on the physical properties of the step structure. Detecting the propagating direction of the scattered TOS can be an alternative approach to retrieve the parameters of the step, which in our case are its height and SWA. To this end, the spatial position of the scattered TOS should be determined firstly. Naturally, the scattered field we are interested is achieved by the differences between the optical field with a step nanostructure and with a flat substrate. The position of the scattered TOS is then settled by monitoring the spatial coordinates of the phase singularity.

A 3D finite-different time-domain (FDTD) model is built for numerical analysis in a commercial FDTD solver (Lumerical FDTD solutions 2020 R2.4). The material of the step structure is set as silicon, the input medium is air, their material index are default values given in the Material library. The wavelength of the three incident Gaussian beams is 633 nm, and they are also the built-in source in the solver, which are typical linearly polarized. Both the propagation direction and the waist of the Gaussian beam can be modified by the user. The adjustment of the propagation direction of three Gaussian beams can control the spatial location of the singularities, and the setting of the waist is equivalent to changing of the NA of the objective to alter the focusing conditions. As a TOS is always distributed within a nanoscale range, the calculating resolution should be fine enough to ensure the final accuracy. The grid size in the step structure region is thus set as 5 nm in x-y plane and 2 nm in z-direction. In the other computational region, the grid size is uniformly set as 25 nm in three directions. Finally, a perfect matching layer (PML) boundary condition is employed for all simulations.

3. Simulation results and discussion

When interaction occurs between the TOS and the step nanostructure, the original TOS will be scattered into the far field at a specific scattering direction. As the TOS possesses a spiral phase around the singularity, the spatial position of the scattered TOS can be retrieved at the singularity thereby. By recording the spatial position of the TOS at various xz-planes, its propagation

trajectory line can be achieved. On this basis, the scattering direction can be retrieved by fitting a straight line with the spatial coordinates of TOSs. The slope of the fitting line refers to the scattered direction of the TOS, which directly reflects the parameters of the step structure.

Given the geometry of the model, the scattering is symmetric along the positive and negative y-axis. Without loss of generality here, we focus on the positive y-axis. To reduce disturbance, the spatial position of the optical source and structure are both fixed in the following analysis. Figure 2(a) shows the process to obtain the trajectory line of the scattered TOS. The spatial location of the scattered TOS is determined by the spiral-shape phase distribution in different cross sections along the y-axis. The yellow circles in the profiles denote the retrieved TOS. By connecting the location of the TOS in each plane, we can obtain its scattering trajectory line. Figure 2(b) shows the trajectories of the scattered TOS with fixed height (633 nm) for various SWAs. As the legends indicate, the yellow line is the trajectory for SWA = 82°, the blue line for 85°, and the red one for 88°. It is obvious that SWAs can influence the location of scattered TOS in each plane and further change its spatial trajectory, in other words, the trajectory line is closely related to the value of the SWA.

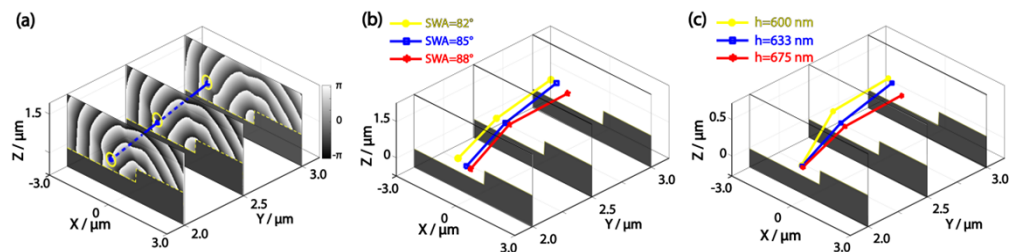


Fig. 2. Spatial trajectory line of scattered TOS by a step nanostructure with different geometrical parameters. (a) The process of tracking the scattered TOS. The trajectory line of the scattered TOS is built by connecting all the position markers along the y-axis. The bottom dark gray region indicates the step structure. (b) The scattered TOS trajectories with step height of 633 nm but various sidewall angles (SWAs). (c) The trajectory line of TOS scattered by the step nanostructure with different heights, while the SWA is 85° for all cases. The simulation results clearly show that the scattering trajectory line is highly dependent on both the height and SWA.

In addition to the SWA, the step height also give rise to changes in propagation direction of the scattered TOS. Figure 2(c) shows the trajectory line of the scattered TOS for different step heights when the SWA is fixed to 85°. In the cross-section of $y = 2.0 \mu\text{m}$, the positions of the scattered TOS for these three heights (675 nm/633 nm/600 nm) almost coincide. For the $y = 2.5$ and $3.0 \mu\text{m}$ plane, the singularity positions are dispersed. Likewise, the trajectory line of the scattered TOSs is then achieved by connecting the location of TOS in each plane. It is clear from these results that the trajectory line shows visible difference in these three cases, which means that the trajectory line is also sensitive to the height of step. We also find that the trajectory line changes fastest along the y-axis, followed by the x-axis, and z-axis, so the change of the trajectory line in xy-plane should be the most obvious one to be considered.

To make a preliminary assessment of the dependence between the scattered TOS and the parameters of the step nanostructure, the SWA and height are swept independently to analyze the scattered behavior of TOS in the xy-plane. In the retrieval of SWAs, the structure height is fixed as 633 nm, and the selected TOS is located at the middle of the step oblique surface. The SWA is swept from 81° to 89° with interval of 1°, and the projection of the 3D trajectories on xy-plane and its fitting curve are plotted in Fig. 3(a). Here, the fitting curves are nearly linear, which reveals that the scattered TOS possesses high directional property. Moreover, the same simulation within a larger calculating region, with the calculating range extended from $\pm 3 \mu\text{m}$ to

$\pm 10 \mu\text{m}$, are performed. The spatial positions of the retrieved TOS show a more linear singularity trajectory in a larger scale (as shown in the Supplement 1). Consequently, the slope of the fitted curves is calculated to get the scattering angles that characterize the directionality of the TOSs. Here, the scattering angle refers to the angle between the fitted straight line and the y-axis.

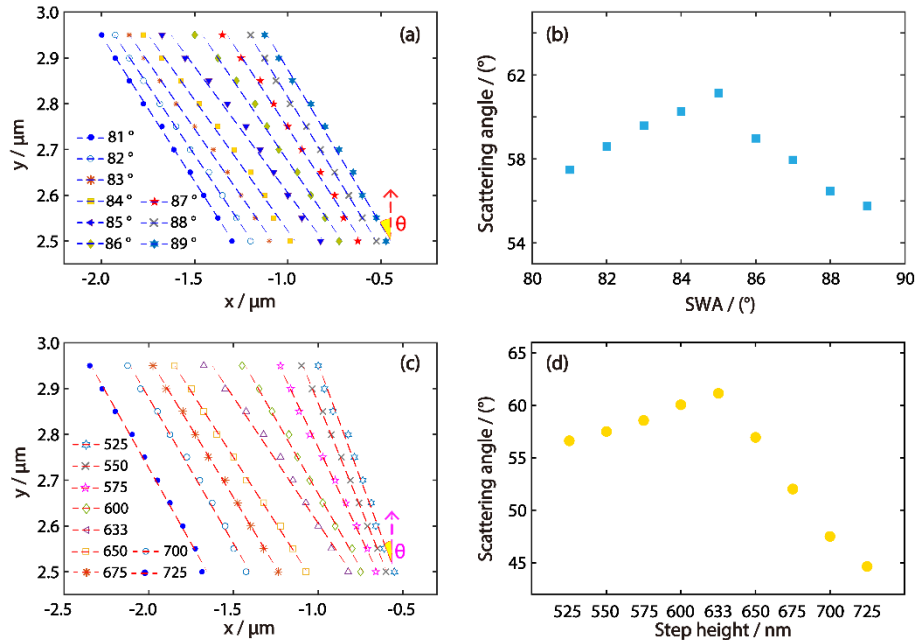


Fig. 3. Properties of the scattered TOS against the step height and SWA. (a) Recorded spatial position of scattered TOS in the xy-plane and the fitting lines for a 633-nm-height step with different SWAs. (b) Retrieved scattering angle of the scattered TOS to the y-axis corresponding to the SWAs shown in (a). (c) and (d) are the corresponding fitting lines and scattering angles for step-structure with different heights.

Figure 3(b) shows the distribution of the scattering angle for different SWAs. We find that different SWAs correspond to different scattering angles, where the maximum value appears at 85° for this condition. The variation range of the scattering angle is typically wider than 5° , which is large enough to be distinguished. For the retrieval of height, the SWA is fixed at 85° , and other eight heights are swept around 633 nm. The selected TOS is still fixed at the middle of the step oblique surface when the height equals to 633 nm. Figure 3(c) and Fig. 3(d) give the fitting curves and scattering angles for different heights, respectively. Like Fig. 3(a) and Fig. 3(b), the changes in height also influence the scattering angle. Each height can be encoded to one scattering angle, and the maximum value appears at 633 nm. Based on these results, one can safely conclude that the scattering direction is highly dependent on changes in SWA and height.

In Fig. 3(b) and (d), the scattering angles both show a tendency of first increasing and then decreasing with respect to the changing of SWA/height, which indicates that the relationship between the scattering angle and SWA/height is not unique. Consequently, only one scattering angle is not sufficient for unique detection. As mentioned in Fig. 2, the trajectory line changes along all three axes, so it is easy to extend the scattering angle calculation onto the other two planes. Figure 4(a) plots the 3D trajectory line of the scattered TOSs, as well as their projection in three planes, for three different SWAs, namely 80° , 85° , and 89° . The height of the structure is still fixed as 633 nm, and the selected TOS is still located at the middle of the step oblique surface, i.e., the same conditions as in Fig. 3(a). It is apparent here that the three trajectories are

spatially independent, and their projections in each plane possesses high directional property. The scattering angles in yz - and xz -plane are defined as the angles between the TOS propagation and the y - and z -axis, as the bright yellow triangles indicate. The data acquisition conditions for Fig. 4(b) are the same as for Fig. 3(c), which shows the 3D trajectories for three different heights, and the corresponding fitting lines in three projection planes. Not only the scattering angles on the xy -plane, but also the scattering angles on the xz - and yz -planes make significant difference. Here we can conclude that the set of three scattering angles provides more freedom in the determination of the structure parameters, which can help to overcome the non-uniqueness problem appeared in Fig. 3 resulting in great potential in precision measurement.

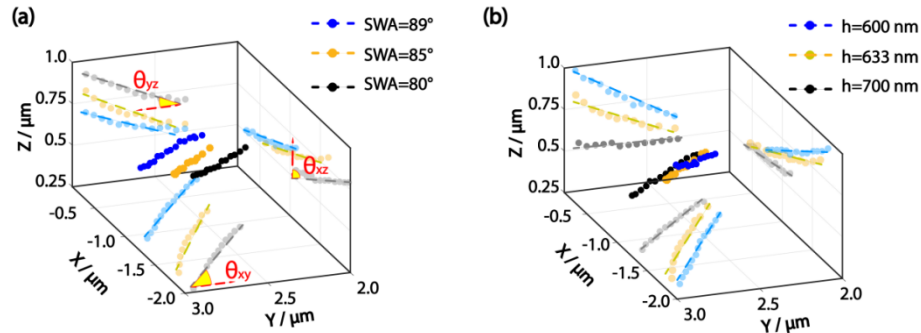


Fig. 4. 3D trajectory line of the scattered TOS against the SWA and step height. (a) The height of the step is fixed at 633 nm, but the SWA varies. The scattering angle in each plane is presented by the bright yellow triangle. (b) The SWA is fixed at 85° with various heights. The trajectory line is projected onto xy -, xz -, and yz -planes, and the fitted curves in each plane exhibit high linearity characteristic.

Finally, Fig. 5 shows the 3D distribution of the scattering angles of the TOSs for step nanostructure with varying parameters. Figure 5(a) depicts the spatial position governed by three scattering angles for different SWAs, and Fig. 5(b) plots the results for different heights. It demonstrates that the scattering angle possesses a dispersed distribution in the 3D space, which means that the parameters of the step structure can be uniquely distinguished by the set of three scattering angles. The spatial distance between two adjacent parameters reflects the degree of discrimination between them. For angle measurement techniques, the distance is large enough to distinguish the difference in the nanostructure parameters.

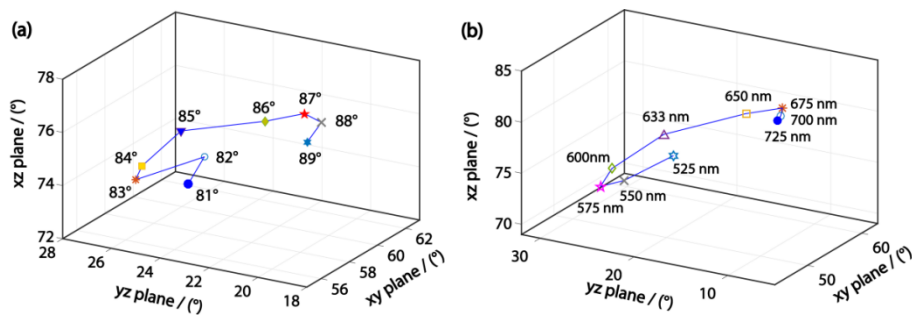


Fig. 5. The unique retrieval of SWA and height of the step structure by using three scattering angle projections. (a) retrieval of the SWA. (b) retrieval of the height.

Since the scattering angle is sensitive to both height and SWA, we need to build a data library of various SWA-height combination. For each SWA-height combination, there will be a unique

set of scattering angles (as shown in Fig. 5(a) and Fig. 5(b)) corresponding to a certain structure. Angle measurement methods are very mature, and it is easy to realize a measurement accuracy up to 1 arcsec [39]. Therefore, the TOS can be perfectly suitable for precision measurement of parameters of the step nanostructures. In addition, since the illuminated area is very small on the sample, roughness should not be a big issue if one considers high quality printed nanostructures. In a previous work of one of the authors [40], they have demonstrated that it is possible to acquire the optical field data that is reliable enough to reconstruct subwavelength features of gratings without considering roughness in the simulations.

In the simulation scenario, the phase information is calculated directly, and the angle information can be obtained by fitting the spatial coordinates of the phase singularity. In experiment, realistically, the phase cannot be measured directly, but one can consider using a reference beam and measuring the intensity after interference [41–46], among which, the Fourier-transform method has been demonstrated to be a robust approach to retrieve the phase distribution of the singularity light field. In experiment, an SLM can be used to generate the three laser beams, which are then incident into an objective lens to generate the focused field with TOSs onto the step structure. The position of step structure can be controlled by a translation platform to align with the TOS. The scattering TOS field along y -direction can be collected by another objective lens on the side of the step structure. Then, the scattering field after the objective lens interferes with an oblique plane wave with the same wavelength to generate the interference fringe field captured by a CCD. Based on the recorded interference field on CCD, the phase distribution of the singularity light field can be retrieved by the Fourier-transform method, and thus the spatial location of the singularity point can be retrieved. Finally, the trajectory of scattered TOS can be obtained by scanning the interference field along the scattering direction with a piezo actuator.

In the proposed method, realistically, the scattering light is relatively weaker compared to the incident light, which constitutes the dominate limitation therein. Thus, a high-sensitivity optical detection system for the scattering light is required in experiment. Besides, the measurement accuracy of the singularity depends highly on the experimental equipment, such as the pixel size of CCD and the angular accuracy of the produced incident beams. In addition, the back-reflected light from the step structure mainly keeps in xz -plane and therefore has a weak influence on the TOS trajectory along y -direction especially in the far-field region. To further eliminate the influence of the reflected light from the step structure, a calibration measurement with a flat substrate is necessary and can be achieved by moving the sample to an area without any structure as the flat reference in experiment.

4. Conclusion

In conclusion, we propose a three-wave interference generated TOS method to retrieve the geometrical parameters of a step nanostructure. Without loss of generality, the step structure is invariant along the y -direction, parallel to the TOS orientation. After interaction with the step structure, the TOS is scattered into the far field, with specific angle depending on the parameters of the step. By detecting the spatial position of the scattered TOS, the scattering angle with the axes are achievable. With this method, it is possible to retrieve both the height and SWA of the structure with high precision. Furthermore, this TOS can also work under a strong focusing mode, which will help to improve the detection accuracy. The TOS, meanwhile, is not limited to the parameter retrieval as described here, but it is expected to play a role in many other broaden scenarios, such as ultra-sensitive sensing, information storage, etc.

Funding. Guangdong Major Project of Basic and Applied Basic Research (2020B030103000); National Natural Science Foundation of China (61935013, 61975128, 62175157); Shenzhen Peacock Plan (KQTD20170330110444030); Science and Technology Innovation Commission of Shenzhen (RCJC20210609103232046).

Disclosures. The authors declare no conflicts of interest.

Data availability. Data underlying the results presented in this paper are not publicly available at this time but may be obtained from the authors upon reasonable request.

Supplemental document. See [Supplement 1](#) for supporting content.

References

1. I.R. Committee, *International Roadmap For Devices And Systems 2020 Edition Lithography*. (IEEE, 2020).
2. M. H. Madsen and P. E. Hansen, "Scatterometry—fast and robust measurements of nano-textured surfaces," *Surf. Topogr.: Metrol. Prop.* **4**(2), 023003 (2016).
3. C. J. Raymond, M. R. Murnane, S. L. Prins, S. Sohail, H. Naqvi, J. R. McNeil, and J. W. Hosch, "Multiparameter grating metrology using optical scatterometry," *J. Vac. Sci. Technol., B: Microelectron. Nanometer Struct.–Process., Meas., Phenom.* **15**(2), 361–368 (1997).
4. O. El Gawhary, N. Kumar, Pereira, S.F. , W.M.J. Coene, and H.P. Urbach, "Performance analysis of coherent optical scatterometry," *Appl. Phys. B* **105**(4), 775–781 (2011).
5. Z. Xi, L. Wei, A. J. Adam, H. P. Urbach, and L. Du, "Accurate Feeding of Nanoantenna by Singular Optics for Nanoscale Translational and Rotational Displacement Sensing," *Phys. Rev. Lett.* **117**(11), 113903 (2016).
6. B. Wang, M. Tanksalvala, Z. Zhang, Y. Esashi, N. W. Jenkins, M. M. Murnane, and C. T. Liao, "Coherent Fourier scatterometry using orbital angular momentum beams for defect detection," *Opt. Express* **29**(3), 3342–3358 (2021).
7. Z. Xi and H. P. Urbach, "Retrieving the Size of Deep-Subwavelength Objects via Tunable Optical Spin-Orbit Coupling," *Phys. Rev. Lett.* **120**(25), 253901 (2018).
8. A. M. Yao and M. J. Padgett, "Orbital angular momentum: origins, behavior and applications," *Adv. Opt. Photonics* **3**(2), 161–204 (2011).
9. Y. Shen, X. Wang, Z. Xie, C. Min, X. Fu, Q. Liu, and X. Yuan, "Optical vortices 30 years on: OAM manipulation from topological charge to multiple singularities," *Light: Sci. Appl.* **8**(1), 90 (2019).
10. T. Ozawa, H. M. Price, A. Amo, N. Goldman, M. Hafezi, L. Lu, and I. Carusotto, "Topological photonics," *Rev. Mod. Phys.* **91**(1), 015006 (2019).
11. Q. Zhan, "Cylindrical vector beams: from mathematical concepts to applications," *Adv. Opt. Photonics* **1**(1), 1–57 (2009).
12. Y. Zhang, J. Shen, C. Min, Y. Jin, Y. Jiang, J. Liu, and X. Yuan, "Nonlinearity-Induced Multiplexed Optical Trapping and Manipulation with Femtosecond Vector Beams," *Nano Lett.* **18**(9), 5538–5543 (2018).
13. T. Brunet, J. L. Thomas, and R. Marchiano, "Transverse shift of helical beams and subdiffraction imaging," *Phys. Rev. Lett.* **105**(3), 034301 (2010).
14. D. Mao, Y. Zheng, C. Zeng, H. Lu, C. Wang, H. Zhang, and J. Zhao, "Generation of polarization and phase singular beams in fibers and fiber lasers," *Adv. Photonics* **3**(01), 014002 (2021).
15. J. Chen, C. Wan, and Q. Zhan, "Engineering photonic angular momentum with structured light: a review," *Adv. Photonics* **3**(06), 064001 (2021).
16. M. Burreli, R. J. P. Engelen, A. Opheij, D. van Oosten, D. Mori, T. Baba, and L. Kuipers, "Observation of polarization singularities at the nanoscale," *Phys. Rev. Lett.* **102**(3), 033902 (2009).
17. H. Laroque, D. Sugic, D. Mortimer, A. J. Taylor, R. Fickler, R. W. Boyd, and E. Karimi, "Reconstructing the topology of optical polarization knots," *Nat. Phys.* **14**(11), 1079–1082 (2018).
18. J. Wang, "Advances in communications using optical vortices," *Photonics Res.* **4**(5), B14–B28 (2016).
19. J. Wang, "High-dimensional orbital angular momentum comb," *Adv. Photonics* **4**(05), 050501 (2022).
20. D. G. Grier, "A revolution in optical manipulation," *Nature* **424**(6950), 810–816 (2003).
21. A. Chong, C. Wan, J. Chen, and Q. Zhan, "Generation of spatiotemporal optical vortices with controllable transverse orbital angular momentum," *Nat. Photonics* **14**(6), 350–354 (2020).
22. C. Wan, Q. Cao, J. Chen, A. Chong, and Q. Zhan, "Toroidal vortices of light," *Nat. Photonics* **16**(7), 519–522 (2022).
23. K. Y. Bliokh, "Spatiotemporal Vortex Pulses: Angular Momenta and Spin-Orbit Interaction," *Phys. Rev. Lett.* **126**(24), 243601 (2021).
24. H. Wang, C. Guo, W. Jin, A. Y. Song, and S. Fan, "Engineering arbitrarily oriented spatiotemporal optical vortices using transmission nodal lines," *Optica* **8**(7), 966–971 (2021).
25. G. Gui, N. J. Brooks, H. C. Kapteyn, M. M. Murnane, and C.-T. Liao, "Second-harmonic generation and the conservation of spatiotemporal orbital angular momentum of light," *Nat. Photonics* **15**(8), 608–613 (2021).
26. G. Gui, N. J. Brooks, B. Wang, H. C. Kapteyn, M. M. Murnane, and C. T. Liao, "Single-Frame Characterization of Ultrafast Pulses with Spatiotemporal Orbital Angular Momentum," *ACS Photonics* **9**(8), 2802–2808 (2022).
27. M. Berry, "Geometry of phase and polarization singularities, illustrated by edge diffraction and the tides," *Proc. SPIE* **4403**, 1–12 (2001).
28. V. A. Pas'ko, M. S. Soskin, and M. V. Vasnetsov, "Transversal optical vortex," *Opt. Commun.* **198**(1-3), 49–56 (2001).
29. P. Liu and B. Lü, "Phase singularities of the transverse field component of high numerical aperture dark-hollow Gaussian beams in the focal region," *Opt. Commun.* **272**(1), 1–8 (2007).
30. K. O'holleran, M. J. Padgett, and M. R. Dennis, "Topology of optical vortex lines formed by the interference of three, four, and five plane waves," *Opt. Express* **14**(7), 3039–3044 (2006).
31. M. R. Dennis, K. O'holleran, and M. J. Padgett, "Singular Optics: Optical Vortices and Polarization Singularities," *Prog. Opt.* **53**, 293–363 (2009).

32. X. Wang, Z. Nie, Y. Liang, J. Wang, T. Li, and B. Jia, "Recent advances on optical vortex generation," *Nanophotonics* **7**(9), 1533–1556 (2018).
33. J. Masajada and B. Dubik, "Optical vortex generation by three plane wave interference," *Opt. Commun.* **198**(1-3), 21–27 (2001).
34. K. W. Nicholls and J. F. Nye, "Three-beam model for studying dislocations in wave pulses," *J. Phys. A: Math. Gen.* **20**(14), 4673–4696 (1987).
35. G. Ruben and D. M. Paganin, "Phase vortices from a Young's three-pinhole interferometer," *Phys. Rev. E* **75**(6), 066613 (2007).
36. X. Cai, J. Wang, M. J. Strain, B. Johnson-Morris, J. Zhu, M. Sorel, and S. Yu, "Integrated compact optical vortex beam emitters," *Science* **338**(6105), 363–366 (2012).
37. N. Biton, J. Kupferman, and S. Arnon, "OAM light propagation through tissue," *Sci. Rep.* **11**(1), 2407 (2021).
38. Z. Xie, T. Lei, F. Li, H. Qiu, Z. Zhang, H. Wang, and X. Yuan, "Ultra-broadband on-chip twisted light emitter for optical communications," *Light: Sci. Appl.* **7**(4), 18001 (2018).
39. W. Ren, J. Cui, and J. Tan, "Parallel beam generation method for a high-precision roll angle measurement with a long working distance," *Opt. Express* **28**(23), 34489–34500 (2020).
40. N. Kumar, P. Petrik, G. K. Ramanandan, O. El Gawhary, S. Roy, S. F. Pereira, and H. P. Urbach, "Reconstruction of sub-wavelength features and nano-positioning of gratings using coherent Fourier scatterometry," *Opt. Express* **22**(20), 24678–24688 (2014).
41. R. Trebino and D. J. Kane, "Using phase retrieval to measure the intensity and phase of ultrashort pulses: frequency-resolved optical gating," *J. Opt. Soc. Am. A* **10**(5), 1101–1111 (1993).
42. R. Barczyk, S. Nechayev, M. A. Butt, G. Leuchs, and P. Banzer, "Vectorial vortex generation and phase singularities upon Brewster reflection," *Phys. Rev. A* **99**(6), 063820 (2019).
43. T. Scharf, M. S. Kim, and H. P. Herzig, "Measuring amplitude and phase of light emerging from microstructures with HRIM," *Proc. of SPIE* **8082**, 80821O (2011).
44. A. Nesci, R. Daendliker, M. Salt, and H. P. Herzig, "Optical near-field phase singularities produced by microstructures," *Proc. SPIE* **4456**, 68–77 (2001).
45. M. Totzeck and H. J. Tiziani, "Phase-singularities in 2D diffraction fields and interference microscopy," *Opt. Commun.* **138**(4-6), 365–382 (1997).
46. M. Eberler, S. Quabis, R. Dorn, and G. Leuchs, "Polarization-dependent effects on phase singularities in the vicinity of sub-lambda structures," *Proc. SPIE* **4777**, 362 (2002).